Reconfigurable Rectifier-Based Detuned Series-Series Compensated IPT System for Anti-Misalignment and Efficiency Improvement

Yang Chen, *Member, IEEE*, Shuangjiang He, Bin Yang, *Student Member, IEEE*, Shuxin Chen, *Member, IEEE*, Zhengyou He, *Senior Member, IEEE*, and Ruikun Mai, *Senior Member, IEEE*

***Abstract*—For an inductive power transfer (IPT) system, mobility is one of the most attractive features, but coupling variations can dramatically affect the system's output. In this article, a reconfigurable rectifier-based detuned series-series (SS) compensated IPT system is proposed to tolerate an extensive coupling range and improve the system efficiency simultaneously. The reconfigurable rectifier, which can operate in a full-bridge rectifier mode or a half-bridge rectifier mode, is used to alter the equivalent ac load from one value to the other so the expected coupling range of the detuned SS topology can be extended. At the same time, the system efficiency is also partly improved because the ac load is changed to get closer to the optimal load of the IPT system. First, a detuned SS IPT system with the reconfigurable rectifier is presented and followed by the analysis of the working modes. Then, a detailed parameter design process and switching control of the reconfigurable rectifier are introduced. Finally, a 400-W prototype was constructed to verify the validity of the proposed method. The experimental results demonstrate that the output power fluctuation of the proposed IPT system is less than 17.5% and the lowest efficiency can be improved from 68.6% to 87.5% with the coupling coefficient varying from 0.1 to 0.4. The proposed method can implement significant antimisalignment and efficiency improvement simultaneously, and it is regarded as a potential solution for low-power IPT applications with high spatial mobility.**

***Index Terms*—Antimisalignment, efficiency improvement, inductive power transfer (IPT), reconfigurable rectifier.**

I. Introduction

INDUCTIVE power transfer (IPT) technology can deliver energy from power sources to loads through magnetic coupling without contact, drawing much attention in recent years. It is widely adopted in numerous applications such as biomedical implants, consumer electronics, electric bicycles, and electric vehicles due to its convenience and flexibility [1], [2], [3], [4], [5].

In an IPT charging application, relatively stable transferred power is one of the critical concerns. The relative position of the primary and secondary coils is arbitrary, and the misalignment usually happens in lateral, longitudinal, and vertical directions. The coupling variation may cause reductions in transmission power and system efficiency.

Control schemes are commonly used in IPT systems to resist coupling variations. A dc–dc converter [6] or variable inductor [7] on the primary or secondary side can regulate the output versus misalignment. Besides, the phase shift control [8] for the inverter or the active rectifier is applied to adjust the output power. These approaches usually require an extensive range of modulation depth against a large coupling variation, which can degrade the efficiency [9]. Moreover, real-time communication is desired if the controller is on the primary side, and an additional dc–dc converter or variable inductor will increase system cost, size, and complexity [10], [11]. Preferred methods to improve displacement tolerance are coil design and compensation topology so the IPT system can hold the inherent characteristic of antimisalignment, simplifying the control schemes.

Concerning coil design, the fundamental principle is to build a relatively uniform magnetic field for the secondary coil. Based on the superposition of magnetic flux, double-D coil, bi-polar pad, and coil array are proposed [12], [13], [14]. Besides, the unsymmetrical coil can also build a uniform magnetic field within a specific range [15]. In addition, using flux cancellation can also create a nearly constant mutual inductance between the primary and secondary coils [16], [17]. However, these methods always have dedicated requirements on the coil design, and most of them only can tolerate either vertical or horizontal misalignment.

Apart from the coil design, a hybrid compensation topology integrated with two topologies with specifically designed coils can alleviate the power drop. The two topologies have opposite trends in outputs versus misalignment so that the total output can remain constant within a wide range of coupling [18]. For example, it can be the combination of *LCC-LCC* and SS topologies with input-parallel/series-output-parallel/series structure [11],

Manuscript received 11 May 2022; revised 27 July 2022; accepted 27 August 2022. Date of publication 6 September 2022; date of current version 18 November 2022. This work was supported by in part by the China Postdoctoral Science Foundation under Grant 2020M683352, in part by the National Natural Science Foundation of China under Grant 51977184, and in part by the Special Fund from the Central Government to Guide the Development of Local Science and Technology in Shenzhen under Grant (2021Szvup122). Recommended for publication by Associate Editor M. Silva. *(Corresponding author: Ruikun Mai.)*

Yang Chen, Bin Yang, Zhengyou He, and Ruikun Mai are with the School of Electrical Engineering, Southwest Jiaotong University, Chengdu 611756, China (e-mail: yangchen@swjtu.edu.cn; yb@my.swjtu.edu.cn; hezy@home.swjtu.edu.cn; mairk@swjtu.edu.cn).

Shuangjiang He is with the Tangshan Institute, Southwest Jiaotong University, Tangshan 063000, China (e-mail: hsjhsj@my.swjtu.edu.cn).

Shuxin Chen is with the School of Electrical and Electronic Engineering, Nanyang Technological University, Singapore 639798 (e-mail: chen1095@e.ntu.edu.sg).

Color versions of one or more figures in this article are available at https://doi.org/10.1109/TPEL.2022.3204592.

Digital Object Identifier 10.1109/TPEL.2022.3204592

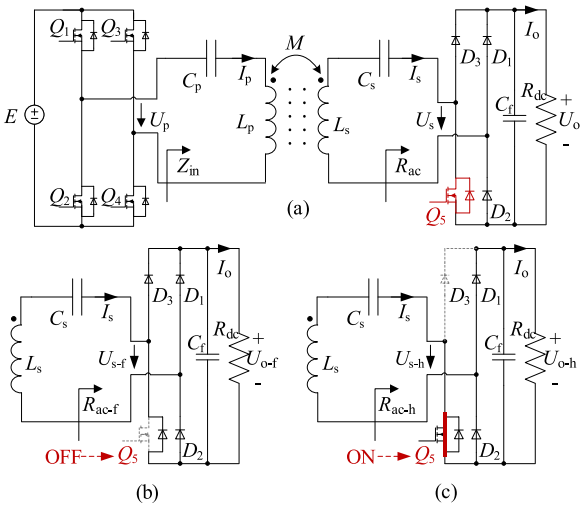

Fig. 1. (a) The reconfigurable rectifier-based SS compensated topology. (b) FBR on the secondary side, and (c) asymmetrical HBR on the secondary side.

[19], or *LCC*-S and S-*LCC* topologies with input-parallel/series-output- series/parallel structure [20], [21]. Furthermore, four-coil couplers are proposed to improve the misalignment tolerance [22], [23]. Nevertheless, these approaches require many passive components, and the design for the coils is rigorous.

As an alternative solution, parameter optimization of compensation topologies can achieve stable transmission power against coupling variation. It does not need a unique coil design, additional coil, or complicated topology. With a dedicated parameter design method, the compensation topology can automatically regulate the primary coil current to keep the power stable within the predetermined coupling range [24]. Topologies, such as SS, *LCC*-S, and X-type are presented with detailed parameter design methods in [10], [24], and [25], where the fluctuation of the output power is no more than 20% with 200% or 250% coupling variation. Moreover, particle swarm optimization is also applied for parameter design [26]. However, the allowable coupling range of these approaches is still desired to enhance.

Reconfigurable topologies are proposed to increase the variable coupling range with relatively constant output [27], [28]. The reconfigurable topology has two transfer power-coupling coefficient (*P*–*k*) curves of two topologies, and switches may be used to alter one topology to the other one, leading to more components involved in these topologies.

Moreover, when the coupling factor changes, the system efficiency may drop because the impedance matching condition is missed. In [29], a new coil IPT system with dual transmitters and dual receivers with integrated decoupling coils is proposed to maintain efficiency versus misalignment. Besides, a novel S-S-*LCLCC* compensated three-coil IPT system is presented in [30] to improve the efficiency stiffness against load variation and misalignment. It would be better if the misalignment tolerance and efficiency were improved simultaneously for the IPT system using a straightforward method.

This article proposes a reconfigurable rectifier-based detuned SS compensated IPT system to resist an extensive coupling range with relatively high efficiency. The reconfigurable rectifier can be a full-bridge rectifier (FBR) or an asymmetric half-bridge rectifier (HBR). It is used to alter the equivalent ac load from one value to the other so the expected coupling range of the detuned SS topology can be extended. With the improvement of the misalignment tolerance, the system efficiency is also partly improved simultaneously because the ac load is changed to get closer to the optimal load of the IPT system. Compared to the prior methods, the proposed approach does not require complicated control, dedicated coil design, or complex topology.

The rest of the article is organized as follows. Section II presents the proposed reconfigurable rectifier-based detuned SS topology and offers a detailed analysis. The parameter design procedure for the IPT system is elaborated theoretically in Section III. In Section IV, a 400-W prototype is constructed to verify the theoretical performance. Finally, the conclusion is drawn in Section V.

II. Theoretical Analysis

A. Proposed Reconfigurable Rectifier-Based Detuned SS Topology

Fig. 1 depicts an SS compensated IPT system with a reconfigurable rectifier. The high-frequency inverter is formed with four MOSFETs (Q_1 - Q_4), where E and U_o are the input and output dc voltage. U_p and I_p are the high-frequency input voltage and current of the SS topology, while the U_s and I_s are the high-frequency output voltage and current. The loosely coupled transformer consists of the primary coil L_p and the secondary coil L_s, and M is the mutual inductance between the two coils. Capacitors C_p and C_s are used to compensate for the inductances of the primary and secondary coils. Three diodes (D_1-D_3), one switch Q_5, and one capacitor C_f compose the reconfigurable rectifier. $R_{\rm ac}$ and $R_{\rm dc}$ are the equivalent ac load and dc load, respectively.

Compared to the traditional FBR, the rectifier diode D_4 is substituted by a switch Q_5. There are two configurable structures in the IPT system, as shown in Fig. 1(b) and (c). When Q_5 is turned OFF, an FBR occurs, and the ac load is noticed as $R_{\text{ac-}f}$. The relationship between the input ac voltage/current and output dc voltage/current of the FBR can be expressed as [9]

$$\begin{cases} U_{s-f} = \frac{2\sqrt{2}}{\pi} U_{o-f} \\ I_{s-f} = \frac{\pi\sqrt{2}}{4} I_{o-f} \end{cases}. \tag{1}$$

Then, the input ac load of the FBR can be derived by using the ratio of $U_{s\text{-}f}$ to $I_{s\text{-}f}$, i.e.,

$$R_{{\rm ac}-f} = \frac{8}{\pi^2} R_{\rm dc}. \tag{2}$$

When Q_5 is kept in the ON state, an asymmetrical HBR can be formed, and the ac load becomes $R_{\text{ac-}h}$. The relationship between the input ac voltage/current and output dc voltage/current of the HBR can be given as [9]

$$\begin{cases} U_{s-h} = \frac{\sqrt{2}}{\pi} U_{o-h} \\ I_{s-h} = \frac{\pi\sqrt{2}}{2} I_{o-h} \end{cases}. \tag{3}$$

Similarly, the ac load of the HBR can be obtained as

$$R_{{\rm ac}-h} = \frac{2}{\pi^2} R_{\rm dc}. \tag{4}$$

According to (2) and (4), it implies that a large or small ac load can be configured flexibly by turning ON or turning OFF switch Q_5.

B. Working Modes Analysis

The fundamental harmonic approximation is employed to analyze the system. According to Kirchhoff's voltage law, the SS topology in Fig. 1(a) can be expressed by

$$\begin{bmatrix} U_p \\ 0 \end{bmatrix} = \begin{bmatrix} j\left(X_{Lp}-X_{Cp}\right)+R_p & -jX_M \\ -jX_M & j\left(X_{\mathrm{Ls}}-X_{Cs}\right)+R_s+R_{\mathrm{ac}} \end{bmatrix} \begin{bmatrix} I_p \\ I_s \end{bmatrix} \tag{5}$$

where

$$\begin{cases} X_{Lp}=\omega L_p,\ X_{Cp}=\frac{1}{\omega C_p},\ X_M=\omega M \\ X_{Ls}=\omega L_s,\ X_{Cs}=\frac{1}{\omega C_s},\ M=k\sqrt{L_pL_s},\ \omega=2\pi f \end{cases}. \tag{6}$$

f and k are the operating frequency and the coupling coefficient.

The secondary capacitor C_s is designed to fully compensate the secondary coil because it can decline the ac–ac efficiency of the SS compensated IPT system if the secondary side has reactance [31]. A detuning design is employed on the primary side for antimisalignment improvement [10], i.e.,

$$X_{Ls}-X_{Cs}=0 \tag{7}$$

$$\alpha=1-\frac{X_{Cp}}{X_{Lp}} \tag{8}$$

where α is called the detuning ratio.

The input impedance Z_{in} and corresponding phase angle θ_{in} can be obtained as

$$\begin{cases} Z_{\mathrm{in}}=\frac{U_p}{I_p}=\frac{X_{Lp}X_{Ls}k^2}{R_{\mathrm{ac}}}+j\alpha X_{Lp} \\ \theta_{\mathrm{in}}=\arctan\left(\frac{\alpha R_{\mathrm{ac}}}{X_{\mathrm{Ls}}k^2}\right) \end{cases}. \tag{9}$$

Substituting (7) into (5), the output power P_{s} of the system can be derived as

$$P_s=\frac{R_{\mathrm{ac}}X_{Lp}X_{Ls}U_p^2k^2}{\alpha^2X_{Lp}^2R_{\mathrm{ac}}^2+\left(X_{Lp}X_{Ls}k^2\right)^2}, \tag{10}$$

which indicates that the output power can be treated as a function of coupling coefficient k ($0<k<1$), namely, $P_{\mathrm{s}}(k)$. By setting the derivative of $P_s(k)$ to 0, we can obtain an inflection point k_{inflec}, i.e.,

$$k_{\mathrm{inflec}}=\sqrt{\frac{\alpha R_{\mathrm{ac}}}{X_{Ls}}}. \tag{11}$$

When $\mathrm{k}<k_{\mathrm{inflec}}$, $P_{\mathrm{s}}'(k)>0$, and when $\mathrm{k}>k_{\mathrm{inflec}}$, $P_{\mathrm{s}}'(k)<0$, so the output power can reach the maximum value P_{smax} at the inflection point k_{inflec}. We have

$$P_{smax}=\frac{U_p^2}{2\alpha X_{Lp}}. \tag{12}$$

In FBR mode, the ac load $R_{\mathrm{ac}\text{-}f}$ is equal to $(8/\pi^2)R_{\mathrm{dc}}$. In HBR mode, the ac load $R_{\mathrm{ac}\text{-}h}$ satisfies $R_{\mathrm{ac}\text{-}h}=(2/\pi^2)R_{\mathrm{dc}}$. The relationship between the two ac loads is $R_{\mathrm{ac}\text{-}f}=4R_{\mathrm{ac}\text{-}h}$. Except for the ac load R_{ac}, other components and input dc voltage E are the same. Then, the key parameters of the output power curves with two modes are given in Table I. With the increase of the ac load, the new inflection point k_{inflec} becomes larger, which means the new power *vs*. coupling (*P*–*k*) curve will move to the right of the original *P*–*k* curve. The two curves are outlined in Fig. 2, where k_{min} and k_{max} are the minimum and maximum values of the allowed coupling variation range.

TABLE I
KEY PARAMETERS OF THE OUTPUT POWER CURVES IN TWO MODES

Key Parameters	FBR Mode	HBR Mode
Ac load	$R_{\text{ac-f}}=\frac{8}{\pi^2}R_{\mathrm{dc}}$	$R_{\text{ac-h}}=\frac{2}{\pi^2}R_{\mathrm{dc}}$
Inflection point	$k_{\text{inflec-f}}=\sqrt{\frac{8\alpha R_{\mathrm{dc}}}{\pi^2X_{\mathrm{Ls}}}}$	$k_{\text{inflec-h}}=\sqrt{\frac{2\alpha R_{\mathrm{dc}}}{\pi^2X_{\mathrm{Ls}}}}$
Maximum power	$P_{\text{smax-f}}=\frac{U_{\mathrm{p}}^2}{2\alpha X_{\mathrm{Lp}}}$	$P_{\text{smax-h}}=\frac{U_{\mathrm{p}}^2}{2\alpha X_{\mathrm{Lp}}}$
Input phase angle	$\theta_{\text{in-f}}=\arctan\left(\frac{\alpha R_{\text{ac-f}}}{X_{\mathrm{Ls}}k^2}\right)$	$\theta_{\text{in-h}}=\arctan\left(\frac{\alpha R_{\text{ac-h}}}{X_{\mathrm{Ls}}k^2}\right)$

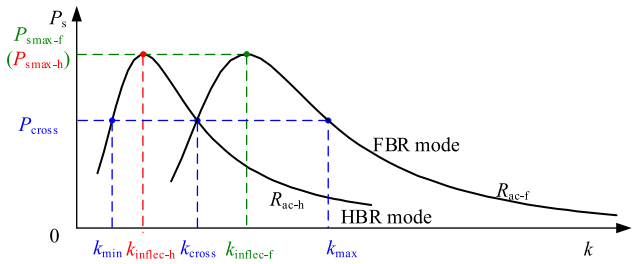

Fig. 2. Two curves of the detuned SS topology in different modes.

As shown in Fig. 2, the two curves have an intersection at k_{cross}, which can be acquired as

$$k_{\mathrm{cross}}=\frac{\sqrt{2\alpha R_{\mathrm{ac}}}}{2\sqrt{X_{Ls}}}. \tag{13}$$

By substituting (13) into (10), the corresponding output power P_{cross} can be obtained, so we have

$$P_{\mathrm{cross}}=\frac{2U_p^2}{5\alpha X_{Lp}}=P_{s-h}\left(k_{\mathrm{min}}\right)=P_{s-f}\left(k_{\mathrm{max}}\right) \tag{14}$$

where

$$k_{\mathrm{min}}=\frac{\sqrt{2\alpha R_{\mathrm{ac}-h}}}{4\sqrt{X_{Ls}}} \tag{15}$$

$$k_{\mathrm{max}}=\frac{\sqrt{2\alpha R_{\mathrm{ac}-f}}}{\sqrt{X_{Ls}}}. \tag{16}$$

If the parameters are appropriately designed, the system can operate at the top of the *P*–*k* curves with the required power fluctuation to cover a large coupling range. The ac load should be altered from one value $R_{\mathrm{ac}\text{-}f}$ to the other value $R_{\mathrm{ac}\text{-}h}$ so the IPT system can hold the small fluctuation part of the two curves. Therefore, on the basis of the abovementioned conclusion, when the coupling coefficient k is located in $[k_{\mathrm{min}}, k_{\mathrm{cross}}]$, the asymmetrical HBR is active; when k grows, and the coupling range belongs to $[k_{\mathrm{cross}}, k_{\mathrm{max}}]$, the FBR operates.

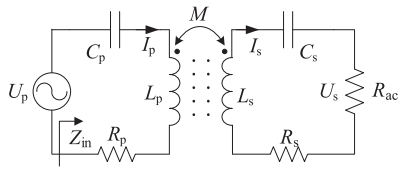

Fig. 3. Equivalent SS compensated IPT system.

III. System Design and Switching Control

A. Design Consideration of the Efficiency

To analyze the system efficiency, the internal resistances of the primary and secondary coils cannot be ignored, which are defined as R_p and R_s, as depicted in Fig. 3.

The efficiency from ac input to ac output can be calculated as

$$\eta = \frac{R_{\mathrm{ac}} X_{Lp} X_{Ls} k^2}{(R_s + R_{\mathrm{ac}})(X_{Lp} X_{Ls} k^2 + R_p R_s + R_p R_{\mathrm{ac}})}. \tag{17}$$

There exists an optimal value $R_{\text{ac-opt}}$, that maximizes (17), and the value is given by

$$R_{\mathrm{ac-opt}} = \sqrt{\frac{R_s}{R_p}(X_{Lp} X_{Ls} k^2 + R_p R_s)}. \tag{18}$$

If the primary and the secondary coils are nearly the same, we have $R_p \approx R_s$. And the product of R_p and R_s is small enough, (18) can be further simplified as

$$R_{\mathrm{ac-opt}} \approx k\sqrt{X_{Lp} X_{Ls}}. \tag{19}$$

According to (19), we can conclude that when the coupling coefficient k changes with fixed ac load, the impedance matching condition is missed, and the efficiency will drop dramatically with a large coupling variation. However, if the value of the ac load R_{ac} is altered to get closer to $R_{\text{ac-opt}}$, it can lead to higher system efficiency [9]. Therefore, in the FBR mode, the ac load $R_{\text{ac-}f}$ is set as

$$R_{\mathrm{ac}-f} \approx k_{\max}\sqrt{X_{Lp} X_{Ls}}. \tag{20}$$

B. Parameter Design

To design the parameters, some system parameters should be predetermined, including the operating frequency f, the inductance of the primary coil L_p, the inductance of the secondary coil L_s, the maximum coupling coefficient $k_{\max}$, and the maximum output power $P_{\max}$.

Then, substituting (16) into (20), we can obtain

$$R_{\mathrm{ac}-f} = 2\alpha X_{Lp}. \tag{21}$$

Combined with (16), (20), and (21), the detuning ratio α is determined as

$$\alpha = \frac{\sqrt{k_{\max}^2 X_{Lp} X_{Ls}}}{2X_{Lp}}. \tag{22}$$

Afterward, according to the following steps to calculate the parameters, the corresponding flowchart is shown in Fig. 4.

1) Use (6) and (7) to calculate the value of the secondary capacitor C_s.

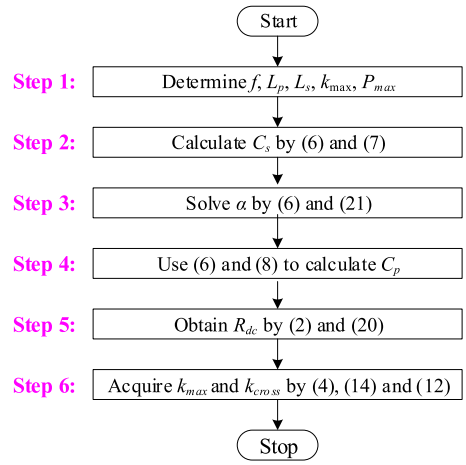

Fig. 4. Flowchart of the parameter design.

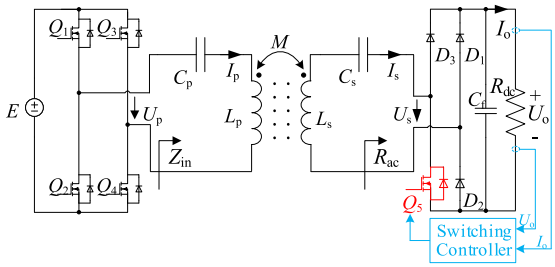

Fig. 5. One implementation of switching between two modes.

2) Use (6) and (22) to calculate the detuning ratio α.
3) Use (6) and (8) to calculate the value of the primary capacitor C_p.
4) From (2) and (21), the dc load R_{dc} can be obtained accordingly.
5) Use (4), (15), and (13) to calculate the minimum coupling coefficient $k_{\max}$, and the intersection k_{cross} of the two curves.

C. Switching Control

The switching between the two modes is decided by the coupling coefficient k. When k is located in $[k_{\min}, k_{\mathrm{cross}}]$ or $[k_{\mathrm{cross}}, k_{\max}]$, the output power range is $[P_{\min}, P_{\max}]$. Instead of estimating the coupling coefficient, the output power is the primary concern so that the output power can be applied to determine the switching time. U_o and I_o are measured to estimate the output power. Fig. 5 illustrates one possible implementation of the switching, where the flowchart of the controller is outlined in Fig. 6. Use U_o and I_o to evaluate the output power P_o. By comparing the estimated P_o with the maximum and minimum power $P_{\min}$ and $P_{\max}$, the switching controller decides the switch Q_5 should turn ON/OFF or stay as it is. After the operation of Q_5, if P_o is still not located in $[P_{\min}, P_{\max}]$, the IPT system should be shut down because k is not within the predetermined coupling range. In addition, the load R_{dc} of the proposed method is required to be fixed, so only the voltage U_o or current I_o is measured to estimate the output power.

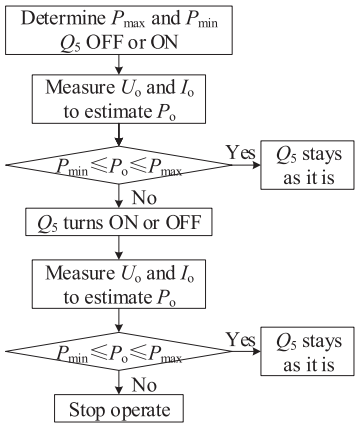

Fig. 6. Flowchart of the controller for the switching.

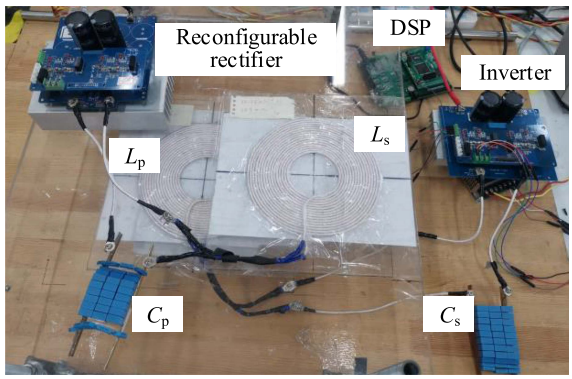

Fig. 7. Experimental prototype.

TABLE II
IPT SYSTEM SPECIFICATION AND PARAMETER VALUES

Description	Symbol	Value
Input dc voltage	E	120 V
Inductance of the primary coil	L_p	38.16 μH
Inductance of the secondary coil	L_s	37.63 μH
Capacitance of the primary capacitor	C_p	13.05 nF
Capacitance of the secondary capacitor	C_s	10.62 nF
System operating frequency	f	250 kHz
Maximum allowable coupling coefficient	k_{max}	0.4
Minimum allowable coupling coefficient	k_{min}	0.1
Intersection of the two curves	k_{cross}	0.2
Dc load	R_{dc}	30 Ω

IV. EXPERIMENTAL VALIDATION

A. Experimental Prototype

To validate the availability of the proposed method, a 400-W IPT system was constructed, as shown in Fig. 7. The MOSFETs $Q_1 - Q_5$ are C2M0080120D, and the rectifier diodes $D_1 - D_3$ are C4D20120D. The dc load R_{dc} is replaced by an electronic load (IT8816B). A digital power analyzer, PW6001 of HIOKI, is used to analyze the power and efficiency of the system. The system parameters in the experiment are given in Table II. Based on the parameter design procedure, the allowable coupling range is from 0 .1 to 0.4. The coupling of the operating region is 0.1–0.2 when switch Q_5 is ON, and that is 0.2–0.4 when Q_5 is OFF.

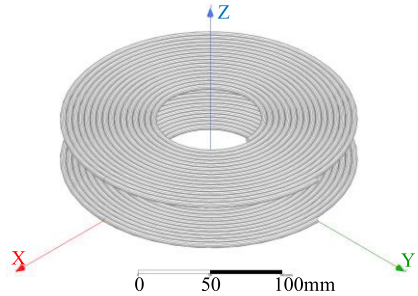

Fig. 8. Simulation model of the circular coils.

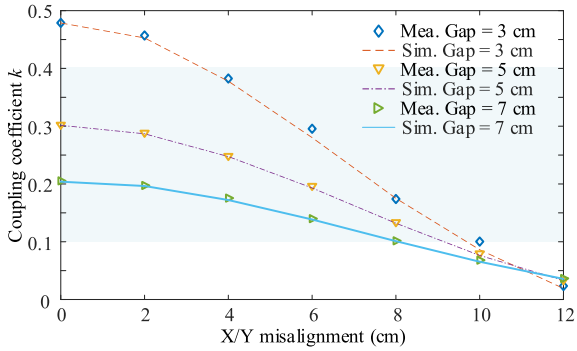

Fig. 9. Measured and simulated coupling coefficients versus horizontal misalignment and air gap.

The primary and secondary coils are both circular coils wounded with 16 turns Litz wire (AWG 43), and the corresponding out radius is 100 mm, as shown in Fig. 8. The coil resistances R_p and R_s are 0.12 and 0.11 Ω, respectively. Since the circular coils are symmetric, the misalignment performances on the X- and Y-axis are the same. The measured and simulated coupling coefficients versus horizontal misalignment and air gap are outlined in Fig. 9. It indicates that the overall tendency of measured coupling variation with misalignment is in good agreement with the simulated ones.

B. Experimental Results

Fig. 10 shows the steady-state experimental waveforms of the output current/voltage of the inverter and the input current/voltage of the reconfigurable rectifier with different coefficient factors, where the load resistance is $R_{dc} = 30$ Ω. In Fig. 10(a)–(c), the reconfigurable rectifier operates in HBR mode and the corresponding coupling coefficients are 0.10, 0.15, and 0.20, respectively. In Fig. 10(d) and (e), the IPT system works in FBR mode and the corresponding coupling factors are 0.2, 0.29, and 0.40 separately. It can be found that the input impedance of the system is inductive, which is beneficial to the implementation of zero voltage switching (ZVS) for the high-frequency inverter. Besides, it can be found that with the drop of the coupling factor, the phase angle of the input impedance of the inverter grows larger, leading to more reactive power. Additionally, Fig. 11 depicts the experimental waveforms of the MOSFET Q_4 in HBR and FBR modes with different coupling factors. It is

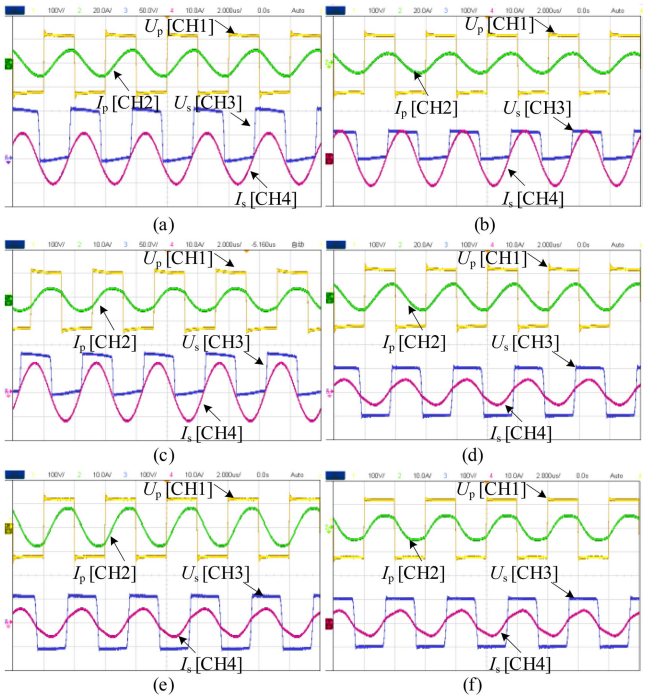

Fig. 10. Experimental waveforms of Up, Ip, Us and Is @ $R_{\rm dc} = 30\ \Omega$. (a) HBR with $k = 0.10$. (b) HBR with $k = 0.15$. (c) HBR with $k = 0.20$. (d) FBR with $k = 0.20$. (e) FBR with $k = 0.29$. (f) FBR with $k = 0.40$.

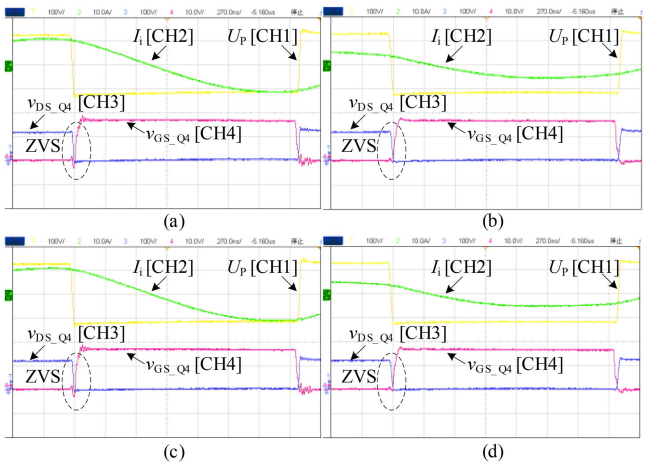

Fig. 11. Experimental waveforms of MOSFET Q_4. (a) $k = 0.1$ in HBR mode. (b) $k = 0.2$ in HBR mode. (c) $k = 0.2$ in FBR mode. (d) $k = 0.4$ in FBR mode, where $v_{\rm DS-}Q4$ and $v_{\rm GS-}Q4$ are the voltage of the MOSFET and corresponding gate drive signal.

apparent that ZVS turn-ON for the semiconductor switches is implemented within the whole allowable coupling range [0.1, 0.4].

Fig. 12(a) and -(b) shows the transient waveforms of switching from the FBR mode to HBR mode and then back to FBR mode. It can be found that the output dc voltage U_o and dc current I_o are nearly constant. When the FBR is changed to the HBR, the voltage U_s is halved while the current I_s is doubled. The reason for the doubled current is that the ac load is altered from $R_{\text{ac-}f}$ ($R_{\text{ac-}f} = 4R_{\text{ac-}h}$) to $R_{\text{ac-}h}$. Fig. 12(c) and (d) are

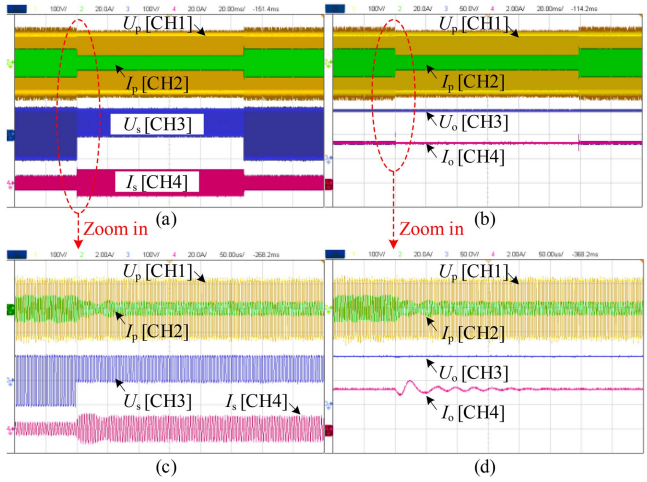

Fig. 12. Transient waveforms of switching between the full-bridge and HBRs. (a) AC voltage/current, (b) DC voltage/current of the reconfigurable rectifier. (c) Zoom-in waveforms of the ac voltage/current. (d) Zoom-in waveforms of the dc voltage/current.

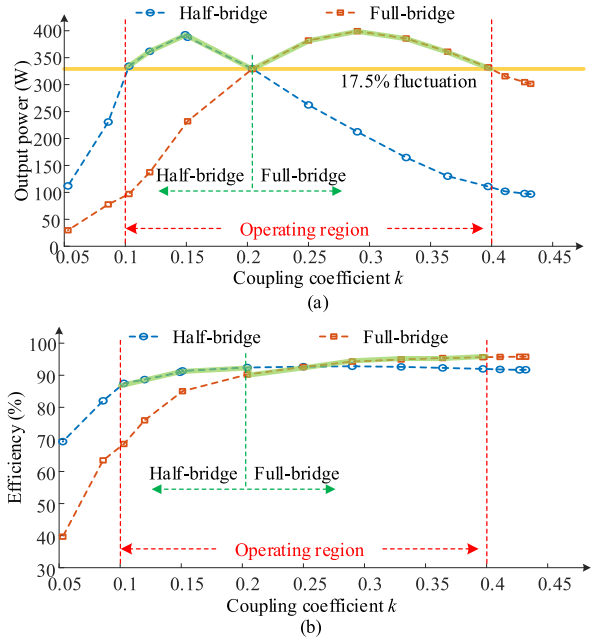

Fig. 13. Measured (a) output power and (b) efficiency with different coupling coefficients in the experiment.

the corresponding zoom-in waveforms from the FBR mode to the HBR mode. Current oscillation can be observed, and it takes around 200 μs from the transient state to go back to the steady state.

The output power and dc–dc overall system efficiency of the IPT system versus misalignment are outlined in Fig. 13. When the coupling range is [0.1, 0.2], the asymmetric HBR is in operation. The maximum power is about 393 W, and the minimum value is around 330 W. When the coupling range is [0.2, 0.4], the FBR is used. The maximum and minimum power is about 400 W and 330 W, respectively. The power fluctuation of the system with the reconfigurable rectifier can be calculated as (400-330)/400 = 17.5%. Nevertheless, if only the HBR (or FBR)

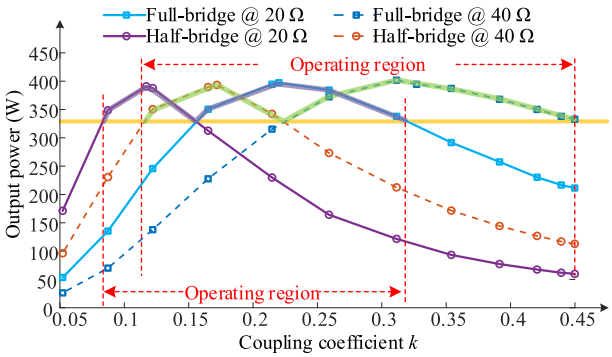

Fig. 14. Measured output power with different loads.

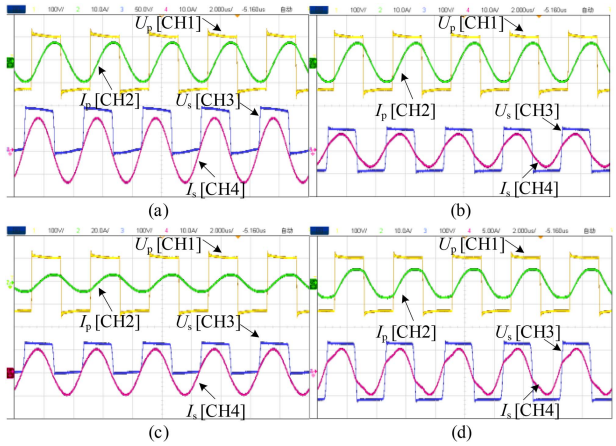

Fig. 15. Experimental waveforms of *Up*, *Ip*, *Us*, and *Is*. (a) HBR with $k = 0.12$ @ $R_{\rm dc} = 20\ \Omega$. (b) FBR with $k = 0.22$ @ $R_{\rm dc} = 20\ \Omega$. (c) HBR with $k = 0.18$ @ $R_{\rm dc} = 40\ \Omega$. (d) FBR with $k = 0.38$ @ $R_{\rm dc} = 40\ \Omega$.

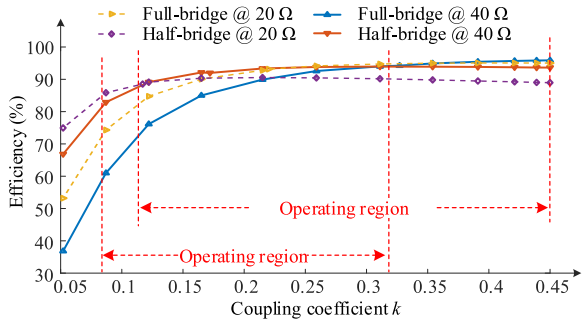

Fig. 16. Measured transfer efficiency with different loads.

works within the coupling range [0.1, 0.4], the power fluctuation is 71.7% (or 75.5%). The proposed method can remarkably improve the antimisalignment ability of the system.

As for the efficiency shown in Fig. 13(b), the efficiency of the system using the HBR is [87.5%, 92.4%] within the coupling range [0.1, 0.2], while the efficiency with the FBR is [68.6%, 90.2%] in the same range. The maximum efficiency improvement is about 19.2% when $k = 0.1$. Likewise, the efficiency of the FBR is [90.2%, 95.6%] within the coupling range [0.2, 0.4], while the efficiency of the HBR is [91.9%, 92.0%]. The maximum efficiency improvement is around 3.6% with $k = 0.4$. Hence, the proposed approach can improve the transfer efficiency of the IPT system with different coupling factors, and the effect is significant with a low coupling factor.

Combining Fig. 9 with Fig. 13, we can obtain the allowed ranges of the horizontal misalignment and air gap with stable output power. For example, the allowed *X/Y* misalignment range is [0 cm, 9 cm] when the air gap is 5 cm; the *X/Y* misalignment range is [0 cm, 8 cm] when the air gap is 7 cm. It should be emphasized that the coupling coefficient is the main concern in the proposed method, and the circular coil is just an example utilized to build the experimental prototype. For different coil pads, the variation tendencies of the coupling coefficient against the misalignment are different. If a larger misalignment range is required, coil structures, such as DD pad [13], three-coil pad [16], and unsymmetrical pad [15] could be applied.

Fig. 14 depicts the measured output power of the IPT system with different loads, which are 20 and 40 Ω, respectively. It demonstrates that with the increase of the load, the *P–k* curve will move to the right, and it will shift to the left with the drop of the load. While the maximum allowed coupling coefficient is still nearly four times the minimum allowed coupling coefficient. Combined with the *P–k* curve under the dc load of 30 Ω, the influence of the changes in load resistance on the maximum output power is relatively small. It should be noticed that if the IPT system is required to operate within the predetermined coupling range, the dc load is preferred to be fixed.

Some representative steady-state experimental waveforms of the output current/voltage of the inverter and the input current/voltage of the reconfigurable rectifier with different coefficient factors and loads are given in Fig. 15. In Fig. 15(a) and (b), the dc load $R_{\rm dc}$ is 20 Ω and the corresponding coupling coefficients are 0.12 (in HBR mode) and 0.22 (in FBR mode). In Fig. 15(c) and (d), the load is 40 Ω and the corresponding coupling coefficients are 0.18 (in HBR mode) and 0.38 (in FBR mode), respectively. As evident from the waveforms, the input impedance of the IPT system is still inductive. Moreover, the corresponding measured transfer efficiency (dc–dc) with different loads is outlined in Fig. 16. We can find that the efficiency is distinctly improved using the proposed method under different loads, especially with a low coupling coefficient, thereby still offering satisfying performance.

C. Discussion and Comparison

If the IPT system does not need precise output and the output is allowed to vary within a certain range, the proposed method can be applied. In that case, there are no additional converters or complicated control. Only the rectifier diode D_4 is substituted by a switch Q_5. It takes advantage of the detuned SS compensation topology with misalignment tolerance, and there is no complicated control in the proposed system. The hardware and software requirements are low compared to traditional control schemes, and it can relieve the control pressure if the control scheme is applied together. Compared to methods of coil design, this approach has no complicated design considerations, and offset directions are arbitrary. Compared to hybrid compensation topologies, the proposed system needs fewer coils or

TABLE III
COMPARISON WITH OTHER METHODS REPORTED IN LITERATURES

Reference	Coil complexity	Coil/ Inductor counts	Capacitor/ Switch counts	Coupling range (percentage change)	Misalignment tolerance distance/cm (percentage)	Fluctuation	Output characteristic	Efficiency	Max. power
[10]	Low	2/0	2/0	0.08–0.2 (250%)	N/A	20%	Constant power	66%–73%	70 W
[11]	High	4/0	6/0	0.15–0.35 (233%)	x-misalignment: -8 ~ +12 (16.3%) y-misalignment: ±16 (40.9%) z-misalignment: ±2 (16.7%)	10%	Constant power	85%–94%	3.3 kW
[18]	High	4/2	6/0	0.1–0.25 (250%)	x-misalignment: ±20 (50%) z-misalignment: -2~4 (26.7%)	10%	Constant voltage	88%–93%	3.5 kW
[19]	High	4/2	6/0	0.15–0.36 (240%)	x-misalignment: ±15 (38.4%) y-misalignment: ±15 (20.3%) z-misalignment: ±2 (16.7%)	10%	Constant power	89%–91.5%	3.3 kW
[20]	High	4/4	8/2	0.1–0.26 (260%)	x-misalignment: ±20 (50%) y-misalignment: ±5 (12.5%) z-misalignment: ±5 (33.3%)	10%	Constant current or voltage	75.1%–93.9%	1 kW
[21]	High	4/1	6/0	0.09–0.23 (255%)	x-misalignment: ±15 (37.5%) y-misalignment: ±15 (37.5%) z-misalignment: -2 ~ 3.5 (23.3%)	10%	Constant voltage	92%–94.5%	3.5 kW
[22]	High	4/1	5/0	0.09–0.26 (288%)	x-misalignment: ±22.5 (50%) z-misalignment: -2~8 (53%)	10%	Constant voltage	87%–93%	3 kW
[23]	High	4/0	4/0	0.1–0.25 (250%)	x-misalignment: ±22.5 (50%) y-misalignment: -3 ~ 5 (11.1%) z-misalignment: -2 ~ 7 (46.7%)	10%	Constant current	92%–96%	3.4 kW
[24]	Low	2/2	3/0	0.14–0.28 (200%)	N/A	20%	Constant power	83.5%–87.5%	90 W
[25]	Low	2/1	3/0	0.16–0.32 (200%)	N/A	20%	Constant power	88.5%–92.6%	450 W
[26]	Low	2/1	3/0	0.2–0.4 (200%)	N/A	12%	Constant voltage	61%–88.7%	110 W
[27]	Low	2/1	3/1	0.1–0.25 (250%)	N/A	10%	Constant power	85.8%–91.7%	400 W
This work	Low	2/0	2/1	0.1–0.4 (400%)	N/A	17.5%	Constant power	87.5%–95.6%	400 W

The fluctuation is difined as: (max. output – min. output)/max. output×100%, where max. and min. represent maximum and minimum.

components, and the coil design is simple. Besides, the proposed method has a more extensive allowable coupling variation range than the parameter optimization method for compensation topology. Compared to the reconfigurable topologies, this approach has fewer components, thereby lower cost. Detailed comparison results are given in Table III. It has high spatial freedom for achieving a relatively constant output power against a large coupling variation.

It should be emphasized that the proposed method is different from [9]. The idea in the literature [9] is only to improve the IPT system's efficiency based on a proper selection between full-bridge and half-bridge modes of the inverter and rectifier. However, this article is to realize the anti-misalignment and efficiency improvement simultaneously using the detuning SS topology and reconfigurable rectifier. The proposed approach is more straightforward, cost-effective, and simpler to control.

Admittedly, the detuned SS topology and reconfigurable rectifier result in much reactive power and active switch. Therefore, the proposed approach is not intended for high-power applications. The key objective of this article is to provide a robust power transfer characteristic and relatively high efficiency versus large misalignments. It is noticed that the proposed method is suitable for low-power applications with relatively constant loads, where steady and sufficient transferred power is the top priority. For example, in applications that are some scenarios where receivers are randomly placed such as lighting or kitchen equipment [24], [27], [32].

V. CONCLUSION

In this article, a reconfigurable rectifier, which can change ac load by altering from the FBR to the HBR, is proposed in the detuned SS compensated IPT system for antimisalignment and efficiency improvement. Complicated control, dedicated coil design, or complex topology is not required. This article revealed that the output power of the detuned SS topology can remain relatively stable at the top of the *P–k* curve within a relatively small coupling range, and by changing the equivalent ac load of the detuned SS topology, a new *P–k* curve could be created. Therefore, taking advantage of the two curves, this article realizes stable output power versus an extensive coupling range by adopting the reconfigurable rectifier. Meanwhile, with the ac load being transformed to be closer to the optimal load, system efficiency is also enhanced since the ac load is changed to get closer to the optimal load of the system. In the experiment, the coupling changes from 0.1 to 0.4, the power fluctuation is less than 17.5%, and the corresponding efficiency range is [87.5%, 95.6%] with the reconfigurable rectifier, while the power fluctuation is larger than 70% and the efficiency range is [87.5%, 92.4%] or [68.6%, 95.6%] with the HBR or FBR. The results indicate that a significant anti-misalignment and a prominent efficiency improvement can be achieved with the help of the proposed approach. The detuned SS topology with the reconfigurable rectifier owning a robust response to a large coupling variation range makes it suitable for low-power IPT systems that demand relatively stable output power under frequent position variation.

REFERENCES

[1] Z. Zhang, H. Pang, A. Georgiadis, and C. Cecati, "Wireless power transfer—An overview," *IEEE Trans. Ind. Electron.*, vol. 66, no. 2, pp. 1044–1058, Feb. 2019.

[2] Y. Chen et al., "Variable-parameter T-circuit-based IPT system charging battery with constant current or constant voltage output," *IEEE Trans. Power Electron.*, vol. 35, no. 2, pp. 1672–1684, Feb. 2020.

[3] L. Qian, K. Qian, Y. Shi, H. Xia, J. Wang, and Y. Xia, "TSV based orthogonal coils with high misalignment tolerance for inductive power transfer in biomedical implants," *IEEE Trans. Circuits Syst. II, Exp. Briefs*, vol. 68, no. 6, pp. 1832–1836, Jun. 2021.

[4] Q. Zhang et al., "Research on input-parallel single-switch wireless power transfer system with constant-current and constant-voltage output," *IEEE Trans. Power Electron.*, vol. 37, no. 4, pp. 4817–4830, Apr. 2022.

[5] W. Li, H. Zhao, S. Li, J. Deng, T. Kan, and C. C. Mi, "Integrated LCC compensation topology for wireless charger in electric and plug-in electric vehicles," *IEEE Trans. Ind. Electron.*, vol. 62, no. 7, pp. 4215–4225, Jul. 2015.

[6] J. M. Miller, O. C. Onar, and M. Chinthavali, "Primary-side power flow control of wireless power transfer for electric vehicle charging," *IEEE J. Emerg. Sel. Topics Power Electron.*, vol. 3, no. 1, pp. 147–162, Mar. 2015.

[7] Z. Zhang, F. Zhu, D. Xu, P. T. Krein, and H. Ma, "An integrated inductive power transfer system design with a variable inductor for misalignment tolerance and battery charging applications," *IEEE Trans. Power Electron.*, vol. 35, no. 11, pp. 11544–11556, Nov. 2020.

[8] A. Berger, M. Agostinelli, S. Vesti, J. A. Oliver, J. A. Cobos, and M. Huemer, "A wireless charging system applying phaseshift and amplitude control to maximize efficiency and extractable power," *IEEE Trans. Power Electron.*, vol. 30, no. 11, pp. 6338–6348, Nov. 2015.

[9] S. Chen et al., "An operation mode selection method of dual-side bridge converters for efficiency optimization in inductive power transfer," *IEEE Trans. Power Electron.*, vol. 35, no. 10, pp. 9992–9997, Oct. 2020.

[10] H. Feng, T. Cai, S. Duan, X. Zhang, H. Hu, and J. Niu, "A dual-side-detuned series–series compensated resonant converter for wide charging region in a wireless power transfer system," *IEEE Trans. Ind. Electron.*, vol. 65, no. 3, pp. 2177–2188, Mar. 2018.

[11] L. Zhao, D. J. Thrimawithana, U. K. Madawala, P. Hu, and C. C. Mi, "A misalignment tolerant series-hybrid wireless EV charging system with integrated magnetics," *IEEE Trans. Power Electron.*, vol. 34, no. 2, pp. 1276–1285, Feb. 2019.

[12] A. Zaheer, H. Hao, G. A. Covic, and D. Kacprzak, "Investigation of multiple decoupled coil primary pad topologies in lumped IPT systems for interoperable electric vehicle charging," *IEEE Trans. Power Electron.*, vol. 30, no. 4, pp. 1937–1955, Apr. 2015.

[13] K. Song et al., "Design of DD coil with high misalignment tolerance and low EMF emissions for wireless electric vehicle charging systems," *IEEE Trans. Power Electron.*, vol. 35, no. 9, pp. 9034–9045, Sep. 2020.

[14] C. Joffe, S. Ditze, and A. Roßkopf, "A novel positioning tolerant inductive power transfer system," in *Proc. 3rd Int. Elect. Drives Prod. Conf.*, 2013, pp. 1–7.

[15] Y. Yao, Y. Wang, X. Liu, Y. Pei, and D. Xu, "A novel unsymmetrical coupling structure based on concentrated magnetic flux for high-misalignment IPT applications," *IEEE Trans. Power Electron.*, vol. 34, no. 4, pp. 3110–3123, Apr. 2019.

[16] Y. Chen, R. Mai, Y. Zhang, M. Li, and Z. He, "Improving misalignment tolerance for IPT system using a third-coil," *IEEE Trans. Power Electron.*, vol. 34, no. 4, pp. 3009–3013, Apr. 2019.

[17] Y. Zhang, S. Chen, X. Li, and Y. Tang, "Design methodology of free-positioning nonoverlapping wireless charging for consumer electronics based on antiparallel windings," *IEEE Trans. Ind. Electron.*, vol. 69, no. 1, pp. 825–834, Jan. 2022.

[18] X. Qu, Y. Yao, D. Wang, S. Wong, and C. K. Tse, "A family of hybrid IPT topologies with near load-independent output and high tolerance to pad misalignment," *IEEE Trans. Power Electron.*, vol. 35, no. 7, pp. 6867–6877, Jul. 2020.

[19] L. Zhao, D. J. Thrimawithana, and U. K.Madawala, "Hybrid bidirectional wireless EV charging system tolerant to pad misalignment," *IEEE Trans. Ind. Electron.*, vol. 64, no. 9, pp. 7079–7086, Sep. 2017.

[20] Y. Chen, B. Yang, Z. Kou, Z. He, G. Cao, and R. Mai, "Hybrid and reconfigurable IPT systems with high-misalignment tolerance for constant-current and constant-voltage battery charging," *IEEE Trans. Power Electron.*, vol. 33, no. 10, pp. 8259–8269, Oct. 2018.

[21] Y. Chen et al., "A hybrid inductive power transfer system with misalignment tolerance using Quadruple-D quadrature pads," *IEEE Trans. Power Electron.*, vol. 35, no. 6, pp. 6039–6049, Jun. 2020.

[22] W. Zhao, X. Qu, J. Lian, and C. K. Tse, "A family of hybrid IPT couplers with high tolerance to pad misalignment," *IEEE Trans. Power Electron.*, vol. 37, no. 3, pp. 3617–3625, Mar. 2022.

[23] R. Mai, B. Yang, Y. Chen, N. Yang, Z. He, and S. Gao, "A misalignment tolerant IPT system with intermediate coils for constant-current output," *IEEE Trans. Power Electron.*, vol. 34, no. 8, pp. 7151–7155, Aug. 2019.

[24] H. Feng, A. Dayerizadeh, and S. M. Lukic, "A coupling-insensitive X-Type IPT system for high position tolerance," *IEEE Trans. Ind. Electron.*, vol. 68, no. 8, pp. 6917–6926, Aug. 2021.

[25] H. Feng, T. Cai, S. Duan, J. Zhao, X. Zhang, and C. Chen, "An LCC-Compensated resonant converter optimized for robust reaction to large coupling variation in dynamic wireless power transfer," *IEEE Trans. Ind. Electron.*, vol. 63, no. 10, pp. 6591–6601, Oct. 2016.

[26] Y. Yao, Y. Wang, X. Liu, Y. Pei, D. Xu, and X. Liu, "Particle swarm optimization-based parameter design method for S/CLC-Compensated IPT systems featuring high tolerance to misalignment and load variation," *IEEE Trans. Power Electron.*, vol. 34, no. 6, pp. 5268–5282, Jun. 2019.

[27] Y. Chen et al., "Reconfigurable topology for IPT system maintaining stable transmission power over large coupling variation," *IEEE Trans. Power Electron.*, vol. 35, no. 5, pp. 4915–4924, May 2020.

[28] Y. Zhang et al., "Misalignment-Tolerant dual-transmitter electric vehicle wireless charging system with reconfigurable topologies," *IEEE Trans. Power Electron.*, vol. 37, no. 8, pp. 8816–8819, Aug. 2022.

[29] A. Hossain, P. Darvish, S. Mekhilef, K. S. Tey, and C. W. Tong, "A new coil structure of dual transmitters and dual receivers with integrated decoupling coils for increasing power transfer and misalignment tolerance of wireless EV charging system," *IEEE Trans. Ind. Electron.*, vol. 69, no. 8, pp. 7869–7878, Aug. 2022.

[30] P. Darvish, S. Mekhilef, and H. A. B. Illias, "A novel S–S–LCLCC compensation for three-coil WPT to improve misalignment and energy efficiency stiffness of wireless charging system," *IEEE Trans. Power Electron.*, vol. 36, no. 2, pp. 1341–1355, Feb. 2021.

[31] R. Mai, Y. Liu, Y. Li, P. Yue, G. Cao, and Z. He, "An Acti-ve-Rectifier-Based maximum efficiency tracking method using an additional measurement coil for wireless power transfer," *IEEE Trans. Power Electron.*, vol. 33, no. 1, pp. 716–728, Jan. 2018.

[32] M. Itraj and W. Ettes, "Topology study for an inductive power transmitter for cordless kitchen appliances," in *Proc. IEEE PELS Workshop Emerg. Technol., Wireless Power Transfer*, 2018, pp. 1–8.

Yang Chen (Member, IEEE) received the B.Sc. degree in electrical engineering and automation and the Ph.D. degree in electrical engineering from Southwest Jiaotong University, Chengdu, China, in 2015 and 2020, respectively.

From December 2018 to December 2019, he was a joint Ph.D. student founded by the China Scholarship Council with the Future Energy Electronics Center, Virginia Tech, Blacksburg, VA, USA. He is currently a Postdoctoral Researcher with Southwest Jiaotong University, Chengdu, China. His research interests include wireless power transfer.

Shuangjiang He received the B.S. degree in electrical engineering and automation from the School of Electrical Engineering, Changsha University of Science and Technology, Changsha, China, in 2019. He is currently working toward the B.Sc. degree with the School of Tangshan Graduate, Southwest Jiaotong University, Tangshan, China.

His research interest includes wireless power transfer.

Bin Yang (Student Member, IEEE) received the B.S. degree in electrical engineering and automation from the School of Electrical and Automation Engineering, East China Jiaotong University, Nanchang, China, in 2017. He is currently working toward the Ph.D. degree with the School of Electrical Engineering, Southwest Jiaotong University, Chengdu, China.

His research interests include wireless power transfer, especially on misalignment tolerance improvement.

Shuxin Chen (Member, IEEE) received the B.Eng. degree in electronic engineering from the Hong Kong Polytechnic University, Hong Kong, in 2015, the Bachelor's degree in microelectronic engineering from the Sun Yet-Sen University, Guangzhou, China, in 2015, and the M.Sc. degree in power engineering and the Ph.D. degree from the School of Electrical and Electronic Engineering, Nanyang Technological University, Singapore, in 2016 and 2021, respectively.

From 2018 to 2019, he was a Visiting Scholar with Future Energy Electronics Center, Virginia Tech, VA, USA. Since 2021, he has been a Research Fellow with Nanyang Technological University, Singapore. His current research interests include wireless power transfer and power converter design and control.

Zhengyou He (Senior Member, IEEE) received the B.Sc. and M. Sc. degrees in computational mechanics from Chongqing University, Chongqing, China, in 1992 and 1995, respectively, and the Ph.D. degree from the School of Electrical Engineering, Southwest Jiaotong University, Chengdu, China, in 2001.

He is currently a Professor with the School of Electrical Engineering, Southwest Jiaotong University. His research interests include signal process and information theory applied to electrical power system, and application of wavelet transforms in power system.

Ruikun Mai (Senior Member, IEEE) received the B.Sc. and Ph.D. degrees in electrical engineering from the School of Electrical Engineering, Southwest Jiaotong University, Chengdu, China, in 2004 and 2010, respectively.

He is currently a Professor with the School of Electrical Engineering, Southwest Jiaotong University, Chengdu, China. His research interests include wireless power transfer and its application in railway systems, power system stability and control.